JOM, Vol. 71, No. 6, 2019
https://doi.org/10.1007/s11837-019-03403-0

Deformation Capacity of a Ternary Magnesium Alloy in a Gas-Forming Process at Elevated Temperatures

P. GUGLIELMI,[1,6,7] A. ARSLAN KAYA,[2] Y. TÜRE,[3] A. ATAMAN,[3] E. ARKIN,[4] D. SORGENTE,[5,6] and G. PALUMBO[1,6]

1.—Department of Mechanics, Mathematics and Management, Politecnico di Bari, Bari, Italy. 2.—Engineering Faculty, Mugla Sıtkı Kocman University, Mugla, Turkey. 3.—Faculty of Engineering, Seyh Edabali University, Bilecik, Turkey. 4.—ASSAN-HANIL Co., Kocaeli, Turkey. 5.—School of Engineering, Università degli Studi della Basilicata, Potenza, Italy. 6.—IFN UOS, Bari, Italy. 7.—e-mail: pasquale.guglielmi@poliba.it

An experimental ternary magnesium alloy, Mg-2Zn-2Ce, has been investigated. The attention was focused on the possibility of using this alloy for an unconventional sheet-forming process based on a flexible medium (gas-forming) for applications where weight-saving and complex shapes are required. Free inflation tests were performed at temperatures ranging from 350°C to 450°C, employing either a constant forming gas pressure or pressure jumps during the same test in order to evaluate the strain rate sensitivity, m, of the material. Interrupted free inflation tests at known dome heights were also conducted to investigate both the strain and the microstructural evolution. In addition, the texture behavior of the alloy was studied after hot rolling, revealing a weak deformation texture. Even though the material was in the as-cast condition, the alloy showed a good deformation capacity and contribution due to grain boundary sliding, indicating a potential for superplastic deformation.

INTRODUCTION

The use of light alloys is becoming increasingly important, especially within the "multi-material approach" adopted by the automotive industry to simultaneously reduce fuel consumption and greenhouse gas emissions.[1] While efforts in developing Mg alloys center around improving strength and/or deformation capacity, unconventional forming processes (such as gas-forming and superplastic forming) are also being explored toward the same goal.[2] In essence, both approaches have their respective potential contributions to circumvent, or at least lessen to some degree, some of the inherent anomalies of Mg.[3]

Thus, different alloying additions and/or approaches in alloying, such as the exploration of dilute multi-element systems,[4] or yet-to-be-discovered multi-element proper systems, can be considered as promising approaches towards the much desired properties that have to come hand-in-hand with economic competitiveness. However, novel processing techniques even with those putative superior alloy compositions will still have their own contributions towards greater improvement of properties and/or combatting the aforementioned anomalies.

In order to achieve a high-performance alloy, selection of the alloying elements in this study were made based on the known-through-the-literature effects on Mg and the stacking fault energy (SFE) in Mg alloys. An ideal alloy design strategy for a better deformation capacity should pursue such alloying elements that do not facilitate the already very active basal plane but instead the pyramidal and/or prismatic slip systems. This way, not only would the deformation capacity of the Mg alloy increase but the texture tendency would also diminish. The same approach would also be expected to improve the potential of at least the deformation hardening mechanism and possibly of the grain refinement following recrystallization.

A broad review on the effects of alloying elements used is beyond the scope of this study, and therefore we will limit our scrutiny to the effects of the alloying elements used in the present research

(Published online February 25, 2019)

(more comprehensive reviews on Mg-RE and Mg-Zn-RE systems have been reported by other authors[5,6]).

It has been long known that Zn imparts strengthening, and Ce, more precisely rare-earth elements (REs), increases deformation capacity while also providing strength.[5–10] A well-known commercial alloy, WE43, may be given as an example, which sheds light on the effects of REs. The increased ductility[11–14] even at room temperature via activating additional twinning planes and the pyramidal slip plane, improved strength[15] and reduced texture are all well established[16] and attributed to the presence of Yttrium and REs.

Cerium has the lowest solubility in Mg compared to the other RE elements. Due to Ce addition, deformation becomes more homogeneous as compared to pure Mg, and deformation and annealing textures weaken up to 0.03 at.% Ce, beyond which concentration this effect levels out.[17] Compared to many alloying elements, including Zn, used in Mg, Ce has the greatest segregation tendency to twin boundaries.[9] Although Zhang et al.[18] pointed out some of the outcomes of this important finding, it also begets the question of what the Ce atoms (as well as Zn) already present in the as-cast condition, if any, on the twinning planes do prior to the twinning itself. The answer should be sought in the changes in the SFE of those planes due to the presence of Ce solute atoms. All RE elements lower all types of SFEs in Mg; the degree of drop relatively lessens as the atomic number of the RE element increases.[18] Through this influence on SFE, the dislocation as well as deformation characteristics change.

Zn is an alloying element of the commercially available AZ series in which Zn acts as a more effective[19] solid solution strengthener as compared to Al (almost twice in concentrated solutions,[20] while also imparting grain refinement[21]).

This work aimed to investigate the deformation properties of a new ternary Mg-2Zn-Ce alloy; more specifically, the behavior of this alloy in a gas-forming process was evaluated. In addition to the metallographic investigation performed both on as-cast and hot-formed alloys, the results of an extensive experimental campaign, based on two different methodologies of free inflation tests at three different temperatures (350°C, 400°C and 450°C), have also been presented. In particular, the attention has been focused on the strain condition (evaluated in terms of dome height (DH) and thickness distribution) obtained after each test and on the evaluation of the *m*-value, by varying both temperature and pressure. In addition, to verify the experimental results, *m*-values calculated by the two different experimental approaches were compared. Finally, with the aim of correlating the equivalent strain rate with the microstructural evolution, interrupted free inflation tests were conducted at the highest temperature levels (400°C and 450°C).

MATERIAL, EXPERIMENTAL SETUP AND PROCEDURES

Material

The Mg-2Zn-2Ce alloy was produced via melting under protective argon atmosphere in steel crucibles using about 3-atm Ar pressure in a special electrical furnace. All alloying additions were made by using the relevant master alloys. Alloy composition based on the average of four different large area analysis at small magnifications using the energy-dispersive x-ray spectroscopy (EDS) module of FEI NOVANANO SEM 650 revealed the alloy composition to be Mg-2.02%Ce-1.90%Zn (wt.%) (nominally Mg-2Zn-2Ce). Chemical compositions of the different phases observed in the microstructures were also determined using the same EDS system. Although approximate chemistries of the precipitates were determined, no attempt was made to establish their absolute stoichiometry or crystal structures.

Experimental Setup and Procedures

Free Inflation Tests

The deformation behavior of the alloy was investigated via free inflation tests conducted at three different temperatures (350°C, 400°C and 450°C) and using a properly equipped universal testing machine (INSTRON 4485). The samples, clamped between the blank-holder and the cylindrical die (diameter: 45 mm; die entry radius: 3 mm), were heated by an electric furnace with three controlled zones.[2] Due to the argon gas pressure, the sample was freely deformed into the die and both the temperature and the DH were continuously acquired using a 6-mm-diameter K-type thermocouple in contact with the dome and connected to a magnetostrictive sensor. Circular blanks (diameter: 80 mm; thickness: 1 mm) were cut from the as-cast blocks by means of wire electrical discharge machining. The sample was firmly clamped between the blank-holder and the die to avoid both gas leakages and the material flow-in.

Free inflation tests were conducted employing two different methods: (1) setting a constant pressure (CP tests) of the gas for each test; and (2) by alternatively switching between two different pressure levels during the same test (jump pressure tests; JP tests). In addition, interrupted CP tests at increasing heights (40%, 65% and 90% of DH at rupture) were conducted.

Hot-Rolling Tests

Due to the prohibitive geometry of the dome-shaped samples to obtain flat samples, the behavior of the alloy in terms of deformation texture was studied on planar samples extracted from hot-rolled parts. Hot rolling was conducted on plates 100 mm long with an initial thickness of 5 mm and going

down to 1 mm in 5 steps at 400°C. Inter-pass heating periods were 5 min long.

Metallographic Investigations

Free inflation test samples were cut in half for the metallographic analysis exploiting the axial-symmetry of the dome-shaped deformed sample, so that the cross-section could be analyzed starting from the dome apex, which experiences the maximum strain level by being stretched in all principal directions, down to the flange area, which remains undeformed due to clamping.

The suitably sized metallographic samples were placed in cylindrical paper molds, covered with epoxy resin and then left to cure for 8 h. Finally, the cross-sections were ground and polished according to the conventional metallographic preparation techniques (use of water was avoided in the last stage of polishing). Etchings, if necessary, were carried out by treating the polished surfaces with dilute picric acid and ethanol solutions for 2 s. Samples were then washed with anhydrous ethanol and immediately dried by blowing air.

RESULTS

Microstructure

A SEM micrograph of the as-cast structure of Mg-2Ce-2Zn alloy is given in Fig. 1.

It can be seen that the Mg-2Zn-2Ce alloy has three types of secondary phases: the coarse type decorating the grain boundaries apparently is composed of two, gray and white contrast, phases. The gray contrast portions of the coarse precipitates at grain boundaries have an approximate stoichiometry of $Mg_{2.5}X_{0.5}$(Zn, Ce), and are relatively the much finer type, while the portions with white contrast, located inside the coarse precipitates, have an average stoichiometry of $Mg_{1.5}X_{0.9}$(Zn, Ce). The very fine precipitates of less than 1 μm in size located within the interiors of the grains showed an approximate stoichiometry of $Mg_4X_{0.04}$(Zn, Ce), as determined by the EDS analysis given in Fig. 2. Hu et al.[22] also reported such a coarse secondary phase in Mg-Ce-Zn-Zr system, albeit with a different stoichiometry, that is $(Mg, Zn)_{12}Ce$.

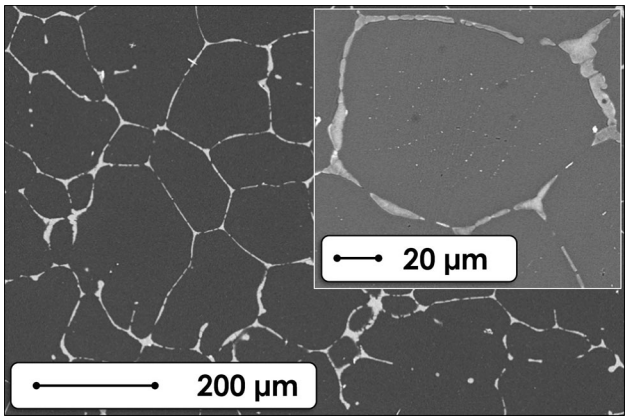

Fig. 1. SEM micrograph of the as-cast structure. Inset shows the presence of intra-granular fine precipitates.

The XRD spectra from the hot-rolled state and the as-cast structure are shown together in Fig. 3, with possible peak positions of α-magnesium indicated. The changes in some of the peak heights have been interpreted as due to the weak texture in the hot-rolled state.

It is worth noting that the stress states in free inflation and rolling are different, the former corresponding to a more complex and multi-axial stress state. Thus, the deductions made from the hot-rolled samples based on XRD data have been tentatively translated in this work to the free inflation samples in the following fashion: it may be possible to envisage a relatively weaker texture and greater non-basal slip in free inflation samples compared to those observed in the hot-rolled one.

Evaluation of Deformation Behavior

Free Inflation Tests up to Failure

Three different temperatures, 350°C, 400°C and 450°C, were adopted for the free inflation tests up to failure, either using the CP or the JP methodology. The pressure levels were chosen in accordance with the temperature so that excessively low strain rates especially at lower temperatures were avoided. Thus, CP tests were conducted adopting the following pressure levels: 1.00 MPa, 1.25 MPa, 1.50 MPa and 1.85 MPa at 350°C; 0.50 MPa, 0.65 MPa, 0.75 MPa, 1.00 MPa and 1.25 MPa at 400°C; and 0.20 MPa, 0.25 MPa, 0.35 MPa, 0.50 MPa and 0.65 MPa at 450°C.

Since a large enough quantity of jumps has to be performed during the JP test, the JP tests were conducted choosing the two lowest pressures levels for each temperature: 1.00 MPa, 1.25 MPa, at 350°C; 0.50 MPa, 0.65 MPa, at 400°C; and 0.20 MPa, 0.25 MPa at 450°C. In order to have large enough durations, the JP tests were conducted changing the pressure alternatively every 100 s.

All the tests were replicated at least two times and, for each temperature and pressure level, the following outputs were evaluated: (1) the maximum dome height, (2) the thickness profiles along the radial path of the formed samples and (3) the m-value. Concerning the m-value, two different approaches were adopted: for CP tests, the m-value was calculated using the Enikeev and Kruglov formulation:[23]

$$m = \ln\left(\frac{p_1}{p_2}\right) / \ln\left(\frac{t_2}{t_1}\right) \quad (1)$$

where t_1 and t_2 are the forming times to reach the height at the pressures p_1 and p_2, respectively; for the JP tests, the formulation proposed by Sorgente et al.[24] was used:

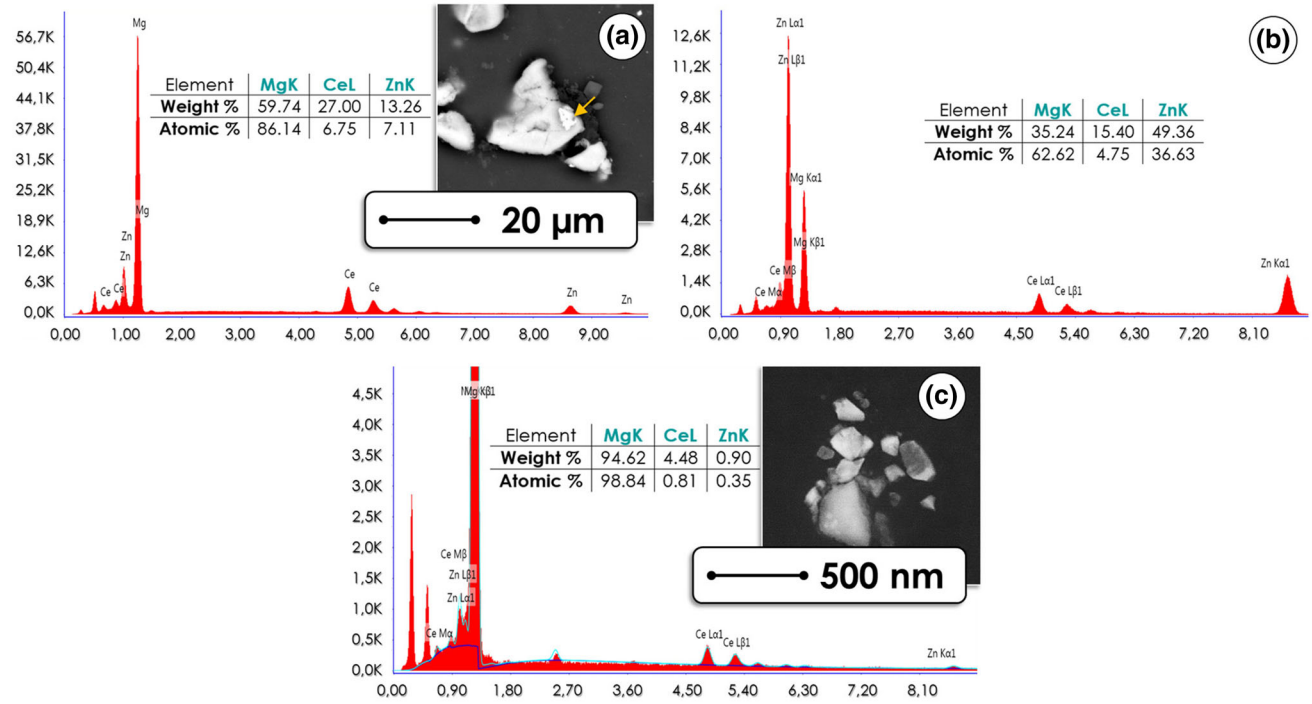

Fig. 2. SEM-EDS microanalysis results from the precipitates at the grain boundaries: (a) coarse areas of gray contrast, and (b) finer areas of white contrast indicated by the arrow; (c) the fine precipitates located in the interiors of the grains in the as-cast structure.

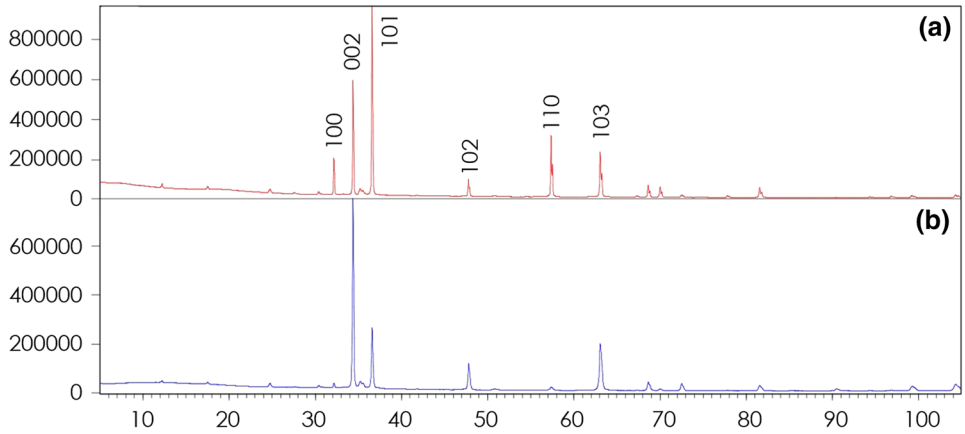

Fig. 3. XRD spectra of (a) the as-cast, and (b) the hot-rolled structure.

$$m = \ln\left(\frac{p_2}{p_1}\right) / \ln\left(\frac{\dot{h}_2}{\dot{h}_1}\right) \qquad (2)$$

where the subscript refers to one of two pressure levels adopted (1: for the low gas pressure level and 2: for the high level); $\dot{h}_1$ and $\dot{h}_2$ are the derivatives with respect to time of DH at a fixed level of pressure.

The results from the CP tests are shown in Fig. 4a, b and c in terms of dome height evolutions (the tests were stopped when the rupture occurred); in the same plots, the m-values at each temperature level (calculated using the data from the tests conducted at the two lowest pressure levels; Eq. 1 have been included.

It should be noted that the DH at which the sample failed increases when increasing the temperature and decreasing the pressure. For example, the dome height at failure increased up to 100% when the temperature was increased from 350°C to 450°C and the pressure was reduced from 1.85 MPa to 0.20 MPa. Figure 4d shows a typical dome-shaped free inflation test sample possessing a characteristic "orange peel" surface for all the test temperatures. The typical failure mode in the free inflation tests were punctures at locations of coarse inclusions or pores formed due to cracking of the

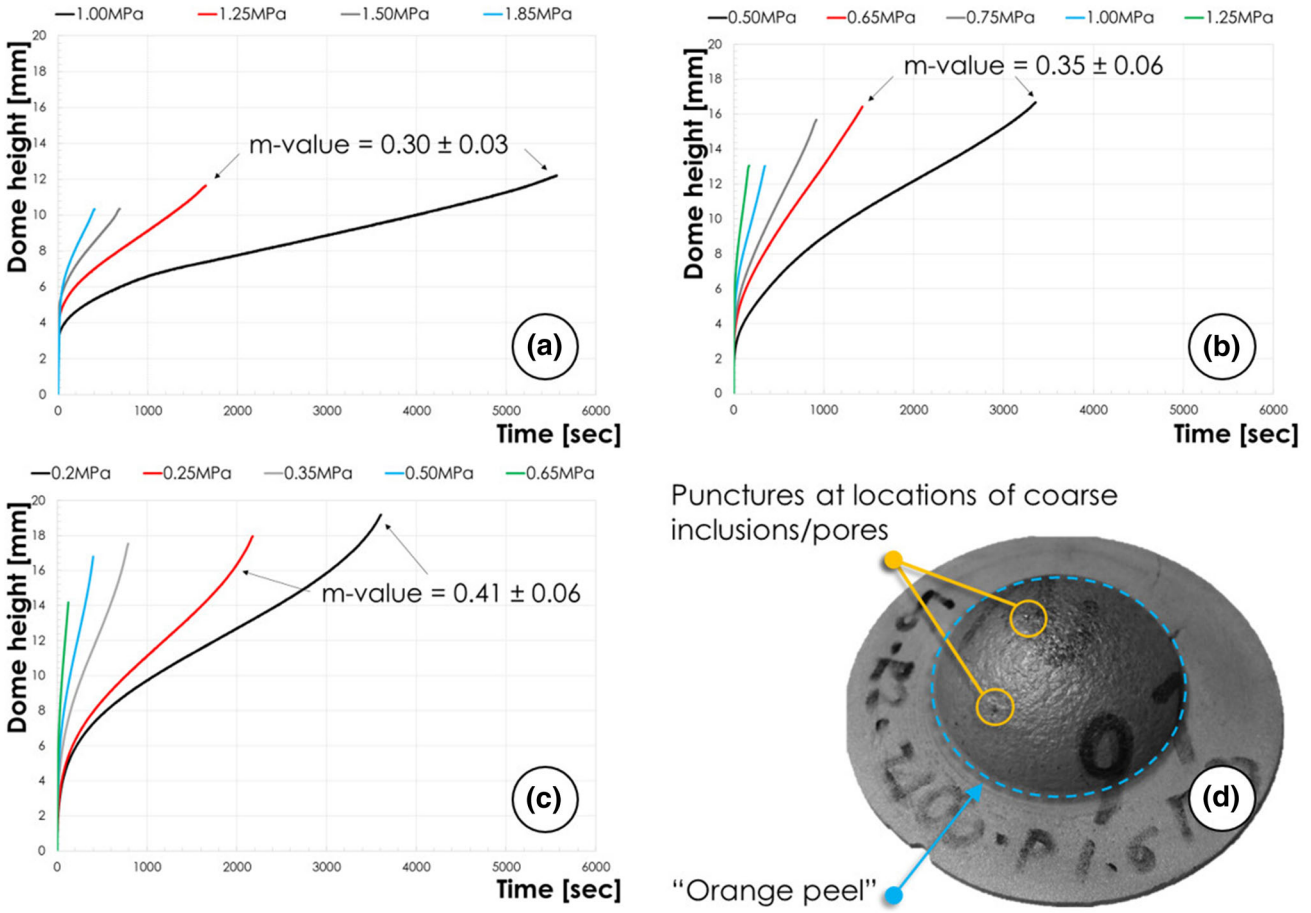

Fig. 4. Dome height versus time curves for CP tests at (a) 350°C, (b) 400°C, (c) 450°C, and photomicrograph (d) showing the external surface of a dome with orange peel appearance and failures at punctures.

coarse secondary phase and the concomitant pressure drop.

The dome evolutions concerning the JP tests have been plotted in Fig. 5a: the jumps between the two pressure levels are clearly visible; in addition, it can be seen that the maximum DH was obtained at 450°C.

For JP tests, the m-value was determined using Eq. 2 at each jump. A graph showing the evolution of the strain rate sensitivity, m, versus time is given in Fig. 5b, c and d. In the same figure, the m-values at each temperature (obtained by averaging all values but excluding the first and the last pressure jump, i.e., the ones immediately after the initial pressure application and the ones just before the rupture) are also shown. It is worth noting that the standard deviations are quite low. From the comparison of m-values calculated using the two approaches (CP tests and JP tests) it can be noted that: (1) irrespective of the adopted methodology, the values are very similar; and (2) according to the temperature, the m-values appear to increase with a linear trend (R^2 = 99.96% for m-values calculated using data from CP tests; R^2 = 99.94% using data from JP tests).

The experimental conditions (temperature and gas pressure) able to determine the highest m-value obtained in the present work are very close to those measured on a commercial Mg alloy (AZ31) in a previous study,[25] thus indicating the good suitability of the alloy proposed in this work (Mg-2Ce-2Zn).

The thickness values were measured along the dome radial cross-path of each formed sample. For all test conditions, the minimum thickness was obviously located at the dome apex, where the material experiences a biaxial stretching state. As a consequence, the equivalent strain at the dome apex could be easily calculated using the thickness measurements (as the natural logarithm of the ratio between the initial thickness and the one measured at the dome).

In Fig. 6a, the maximum equivalent strain at the dome of the samples tested using the CP method has been plotted as a function of pressure and for all temperature levels. It can be noted that the strain linearly decreases when increasing the pressure; on the other hand, the trend is reversed when the temperature effect is considered.

Finally, the thickness distributions along the radial path of the samples from the tests performed

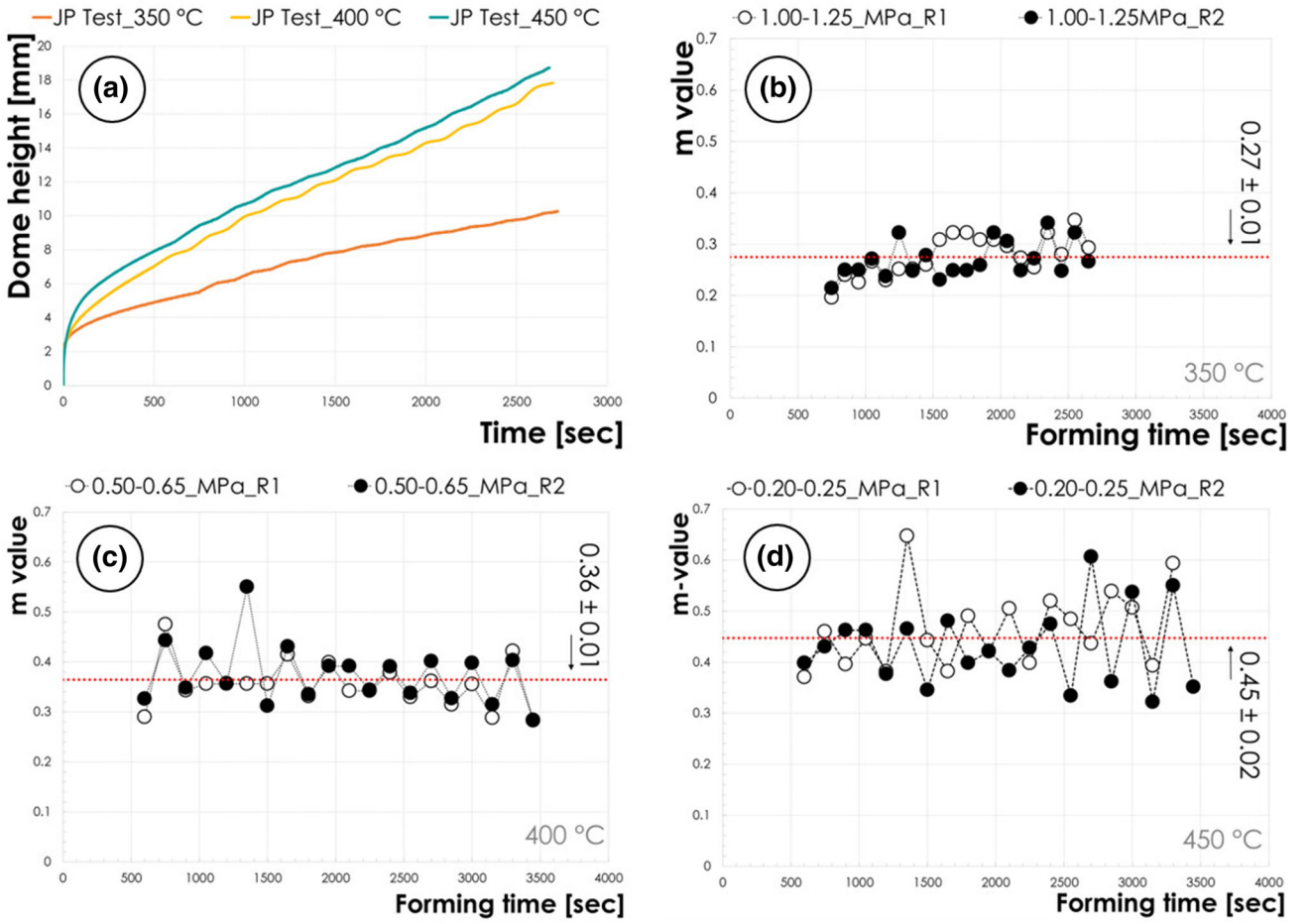

Fig. 5. Dome height versus time curves for JP tests: (a) *m*-values at each jump for the tests conducted at (b) 350°C, (c) 400°C and (d) 450°C.

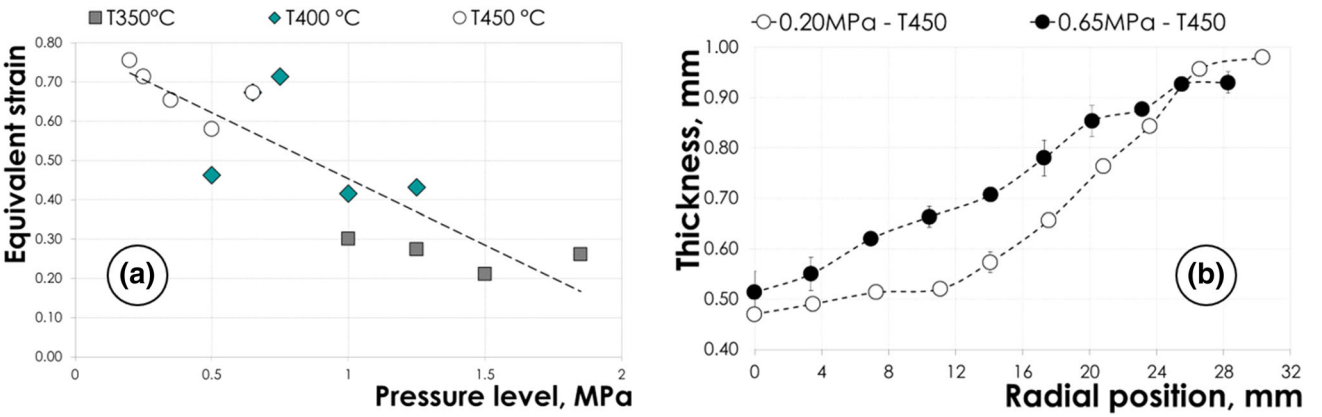

Fig. 6. Evaluation of the equivalent strain at the dome apex according to temperature and pressure (a) for the CP method; thickness variations along the dome radial cross-sections (b) for the CP method at 450°C.

at 450°C employing the highest and the lowest pressure levels are shown in Fig. 6b. It should be noted that the lower the pressure, the higher the strain (see Fig. 6a) achieved. It is also worthy of note that, when decreasing the forming pressure, a greater thinning was observed along the deformed sheet (Fig. 6b). This was consistent with the greater dome height achieved in the sheet formed at the lowest pressure values. The maximum thinning values, i.e., the lowest thickness, at the dome apex for the two tests shown in Fig. 6b were close to each other. A greater uniformity in the thickness distribution was found, especially in the region close to the dome apex, in the specimen deformed with the lowest pressure value (0.2 MPa). This behavior could be related to the effect of the strain rate on the *m*-value

and, consequently, on the ability of the material to exhibit a diffuse necking and a higher ductility. Thus, it can be speculated that, at a specific temperature, the material has the highest m-value at the lowest strain rate values explored in this work. Although the thickness profiles of the samples tested at 350°C and 400°C have not all been given, this observation was valid for all test conditions.

Interrupted Free Inflation Tests

Interrupted CP tests were used to determine the thickness distribution and to observe the evolution of the microstructure at different strain levels. They were conducted up to intermediate levels of the DH at rupture (40%, 65% and 90%) setting two different process conditions (temperature/gas pressure): 400°C/0.75 MPa and 450°C/0.5 MPa.

As depicted in the graph in Fig. 7, the strain at the dome increases during the test according to a linear trend: the strain rate the material experiences at the dome when setting the two different pressure levels can be thus assumed to be the slope of the linear trend which interpolates the strain levels (3.72E−04 s^{-1} and 8.67E−04 s^{-1}, respectively).

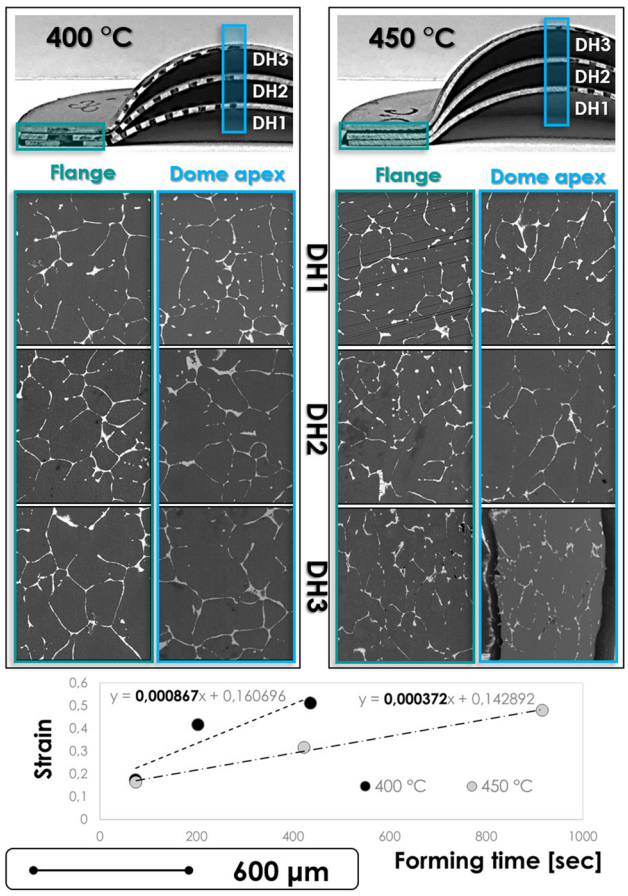

Fig. 7. Micrographs of the region of the dome and of the flange extracted from the samples tested at 400°C/0.75 MPa and 450°C 0.5 MPa up to different DH: 40%, 65% and 90% (scale bar shown at the bottom left).

The microstructural evolution at the three deformation steps is also included in Fig. 7. In particular, two different zones were analyzed: the dome apex, where the deformation was maximum, and the flange, where the strain level was almost zero and only the effect of the temperature was present.

For each temperature investigated, it was observed that the coarse secondary phase appeared to have fragmented during inflation. As evident in the SEM micrographs in Fig. 7, this phenomenon was much more pronounced at the dome, where the strain was maximum, and even present in the intragranular small precipitates in the vicinity. The brittle nature of this second phase is already apparent in the SEM micrograph of the as-cast structure given in Fig. 1, as the metallographic preparation introduced some cracking in the coarse grain boundary phase. In many areas, cavities (pores) between the fragments of this phase were observed to have formed between the fragments of what was previously a single particle (Fig. 8a).

Twinning was not observed in any of the free inflation or rolling samples. Moreover, considering the different deformation temperatures employed, there was no discernible grain size change in any of the samples as compared to the initial as-cast state. It should also be noticed that the grains appeared to show little or no elongation, except for the apex region, in the direction of increasing deformation levels from the flange to the dome apex.

DISCUSSION

The studied alloy with the nominal composition Mg-2Ce-2Zn showed interesting features. Despite the fragmentation of the coarse second phase particles located at the grain boundaries, the formation of cavities between those fragments and the lack of twinning, the good deformation capacity in the as-cast condition and the high m-value are issues that need to be addressed. All the tests were terminated due to point-like punctures rather than tearing, most probably on oxide inclusions or expansion of the pores formed between the fragmented coarse second phase particles located along the grain boundaries.

The Mg-Zn-Ce system was also studied by Mackenzie and Pekguleryuz.[26] Despite the compositional similarity of their material with the one used in our work, they made no reference to the presence of secondary phase(s). They reported weakened and non-basal texture components revealed by EBSD. Contrary to our observations, they also claimed twins based on light microscopy images obtained after deformation at 400°C. However, twins in the images given in that report are not discernible at all, casting doubt on the claim in terms of their existence. On the other hand, their report supports our findings in terms of a weak texture.

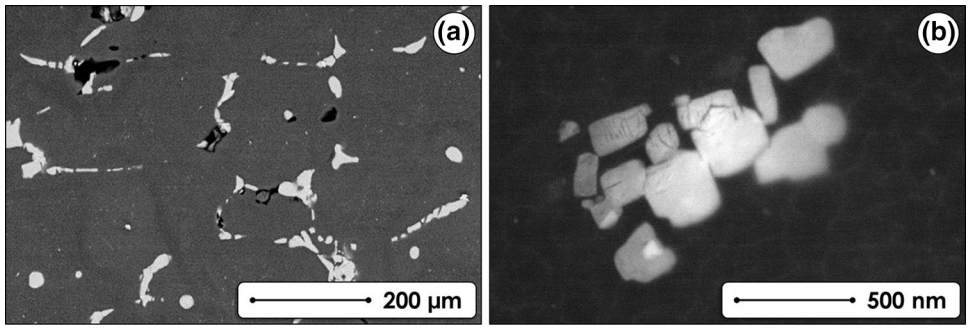

Fig. 8. SEM micrographs of the dome apex zones: cavities generated between the fragments of the grain boundary second phase particles at 450°C (a) and fragmentation of the intergranular fine precipitates (b).

The texture behavior of the composition studied may be assessed indirectly in this work based on the XRD peaks of the α-magnesium matrix from the hot-rolled sample (Fig. 3). Having said that, it can be readily noticed that the peak heights appeared to have changed when spectra of the as-cast and the hot rolled samples are compared. For instance, the relative intensities of the (002) and (101) peaks reversed, the (002), (102) and (004) counts increased, while the intensities of the (100), (101) and (110) planes drastically reduced in the hot-rolled state.

He considerable increase in the intensity of the (002) basal plane can be taken as a strong indication for the existence of a basal texture to some degree. Corresponding decreases in the intensities of especially (100) and (110) planes that make 90° with the basal planes further confirms the crystal orientations in general, indicating that the basal planes are aligned in the rolling direction and parallel to the sample surface describing texture. On the other hand, the dramatic decreases in the intensity of the (101) pyramidal and (110) prismatic planes by about 80% and over 90%, respectively, seem difficult to explain with the increase in the intensity of the (002) basal plane by only about 30%.

Even though evolution of this basal texture can account for some of the decrease in the intensity of the (101) plane, a strong contribution due to the accumulation of dislocations on these pyramidal and prismatic planes, thus bending the crystal and taking these planes out of diffracting condition, can also be envisaged. Therefore, non-basal dislocation mechanisms can reasonably be assumed to have operated, as supported by others in the literature.[16] The observed deformation capacity of this alloy in free inflation tests, despite the absence of twinning, can also be taken to testify for this suggestion.

Admittedly, the stress states in free inflation and rolling are different, the former corresponding to more complex and multi-axial stress states. Thus, the deductions made from the hot-rolled samples based on XRD data may be tentatively translated to the free inflation samples in the following fashion: it may be possible to envisage a relatively weaker texture and greater non-basal slip in free inflation samples compared to those observed in hot-rolled ones.

The deformation capacity observed in the free inflation tests apparently has some contribution from grain boundary sliding (GBS) mechanism as well. The high m-value can also be taken as a strong indication of this proposal.

However, further support can also be found upon close examination of the fragmented grain boundary precipitates. Cavities located between the fragments and the close morphological fitting of the fragment facets with some degree of rotations strongly suggested that the neighboring matrix grains had made relative movements during the free inflation tests. Furthermore, the grain morphologies showed very little elongation except for the dome apex, where the maximum deformation took place. Also considering the absence of twinning, should the GBS be negligible as a deformation mechanism, prominent elongations in the grains would have been inevitable. In a parallel line of thinking, the lack of readily noticeable grain elongations rules out bulk diffusion (viscous flow) as yet another deformation mechanism given the test conditions employed.

The high m-value of the experimental Mg-2Ce-2Zn alloy may be attributed to the short-range interactions of dislocations with the relatively larger size of the solute atoms, Ce and Zn, as compared to that of Mg, as well as to the presence of intra-granular fine precipitates. A comparison of the observed high m-value with that of a well-established alloy, AZ31, may be indicative. El-Morsy et al.[27] reported a superplastic behavior at a strain rate value of about 5E−04 s^{-1} for an AZ31 Mg alloy at 400°C, when the alloy showed an m-value of 0.45. It should be born in mind that the strain rates during the tests conducted in our study were even faster than the conventional strain rates permitting GBS.[22] Although the investigated alloy was in as-cast condition and having a coarse-for-superplastic-behavior grain size, namely about 100–200 μm, it can be said that the Mg-2Ce-2Zn alloy showed a good potential for superplastic deformation, as is also evident from the calculated m-value which was

higher than the conventional limit of 0.3.[27] Furthermore, the material's ability to maintain the grain size and shape were taken as indications that would support this ability.

The resistance to grain coarsening in this alloy can be attributed to the presence of grain boundary precipitates. This feature should also be considered highly useful in superplastic-forming conditions.

In seeking ailments for the anomalous behavior of Mg alloys, e.g., maintaining the deformation texture even after recrystallization, special processing conditions can also be helpful. For example, the forming method employed in this study, gas-forming, would create a multi-axial stress distribution in the material. Especially, hot deformation methods, if coupled with alloy systems that promote random formation of recrystallized grains, can be highly effective in eliminating the post-deformation texture. Although the texture of the free inflation samples was not directly investigated, the Mg-2Ce-2Zn system, in this regard, probably has little, if any, tendency to develop severe texture. Good deformation capacity of this alloy, even in the absence of twinning and predisposition for a superplastic deformation mechanism, indicates that the initial random grain orientation of the as-cast structure was preserved. Furthermore, the presence of grain boundaries as well as intra-granular precipitates could be considered as potential nucleation sites for the formation of randomly oriented new grains during a recrystallization process as a valuable feature of the alloy to eliminate texture, if born.

The effects of Ce and Zn have been well established in the literature. Less than 0.025 at.% Ce addition does not create solute solution strengthening, while increasing deformation capacity considerably due to increased non-basal slip.[28] Low concentration, e.g., 0.2 mass percentage Ce addition, without changing the c/a ratio was still observed to give rise to increased ductility as well as yield strength. Ce has also been reported to delay dynamic recrystallization, possibly due to a reduced diffusion rate, thus leading to lower ductility at high temperatures.[29] Some studies have further indicated that Zn, in low concentrations, created short range order as an additional strengthening mechanism.[30,31] When in solid solution, it is said to facilitate the prismatic slip[32] while suppressing twinning with its increasing concentrations.[33] Zn has also been reported to segregate to the existing twin boundaries, effectively pinning them.[34] According to the data presented in an ab initio study by Shang et.al.[35] Zn has no direct influence on the *twinnability* of Mg. Sandlöbes et al.[18] based on the highly positive effects of yttrium, when developing a similarity-to-yttrium index for each alloying element addition to Mg, assigned a figure of 0.743 for Zn, in terms of increasing the SFE of the basal plane while reducing the SFE for the additional slip systems.[18] In the light of the above, despite the apparent lack of twinning, the good deformation capacity of the alloy studied could reasonably be attributed to the presence of the alloying elements, Ce and Zn. The mechanism of this enhancement can be related to the changes in SFE of the prismatic, and perhaps the pyramidal, slip planes. Thus, based on the literature as well, it can be said that both Ce and Zn enhance deformation capacity via promoting non-basal slip and weaken the basal texture.

CONCLUSION

The experimental Mg-2Zn-2Ce alloy, even though in as-cast condition, showed good deformation capacity in free-inflation tests conducted at different temperatures, failure mode being the point-like punctures rather than tearing, most probably at locations of coarse inclusions or expansion of pores created due to cracking of the second phase particles. Twinning was not observed at all while some evidence existed for contributions from non-basal slip as well as GBS.

It was shown by observations after free inflation tests that the alloy had a resistance to grain coarsening. This grain size stability together with the m-values higher than 0.3 and the accompanying strain rate values varying between 3.72E−04 s^{-1} and 8.67E−04 s^{-1} suggested a potential superplastic behaviour of the alloy with industrially applicable forming times, gas pressures and temperatures.

ACKNOWLEDGEMENTS

The authors gratefully acknowledge the financial support for this work provided by TUBITAK and CNR-Italy under the Project Number 213M535. We also acknowledge the support provided by the Turkish Ministry of Science, Industry and Technology under the SANTEZ Project 0286.STZ.2013-2. Some of the experimental activities related to this work were able to be carried out thanks to the facilities of the TRASFORMA network, funded by Regione Puglia, Italy, and ILTEM of Dumlupinar University, Turkey.

REFERENCES

1. W.J. Joost, *JOM* 64, 1032 (2012).
2. D. Sorgente, G. Palumbo, A. Piccininni, P. Guglielmi, and L. Tricarico, *Int. J. Adv. Manuf. Technol.* 90, 1 (2017).
3. M.O. Pekguleryuz, K. Kainer, and A.A. Kaya, eds., *Fundamentals of Magnesium Alloy Metallurgy* (Amsterdam: Elsevier, 2013).
4. S. Sandlöbes, M. Friák, Z. Pei, J. Neugebauer, and D. Raabe, *Sci. Rep.* 7, 1 (2017).
5. S. Tekumalla, S. Seetharaman, A. Almajid, and M. Gupta, *Metals* 5, 1 (2014).
6. R.K. Mishra, A.K. Gupta, P. Rao Rama, A.K. Sachdev, A.M. Kumar, and A.A. Luo, *Scr. Mater.* 59, 562 (2008).
7. A.A. Luo, R.K. Mishra, and A.K. Sachdev, *Scr. Mater.* 64, 410 (2011).
8. J. Zhang, Y. Dou, and H. Dong, *Scr. Mater.* 89, 13 (2014).
9. J. Zhang, Y. Dou, and Y. Zheng, *Scr. Mater.* 80, 17 (2014).
10. S. Tekumalla, S. Seetharaman, N.Q. Bau, W.L.E. Wong, C.S. Goh, R. Shabadi, and M. Gupta, *J. Eng. Mater. Technol.* 138, 031011 (2016).
11. S. Sandlöbes, S. Zaefferer, I. Schestakow, S. Yi, and R. Gonzalez-Martinez, *Acta Mater.* 59, 429 (2011).

12. S. Sandlöbes, M. Friák, S. Zaefferer, A. Dick, S. Yi, D. Letzig, Z. Pei, L.F. Zhu, J. Neugebauer, and D. Raabe, *Acta Mater.* 60, 3011 (2012).
13. M.R. Barnett, *Mater. Sci. Eng. A* 464, 8 (2007).
14. B.L. Wu, Y.H. Zhao, X.H. Du, Y.D. Zhang, F. Wagner, and C. Esling, *Mater. Sci. Eng. A* 527, 4334 (2010).
15. D.R. Lide, *Handb. Chem. Phys.* 53, 2616 (2003).
16. E.A. Ball and P.B. Prangnell, *Scr. Metall. Mater.* 31, 111 (1994).
17. A. Imandoust, *J. Mater. Sci.* 52, 1 (2017).
18. S. Sandlöbes, Z. Pei, M. Friák, L.-F. Zhu, F. Wang, S. Zaefferer, D. Raabe, and J. Neugebauer, *Acta Mater.* 70, 92 (2014).
19. C. Shaw and H. Jones, *Mater. Sci. Eng. A* 228, 856 (1997).
20. Y. Guyot, I. Papantoniou, Y.C. Chai, S. Van Bael, J. Schrooten, and L. Geris, *Biomech. Model. Mechanobiol.* 13, 1361 (2014).
21. C.S. Roberts, *Magnesium and Its Alloys* (New York: Wiley, 1960).
22. L.F. Hu, Q.F. Gu, Q. Li, J.Y. Zhang, and G.X. Wu, *J. Alloys Compd.* 741, 1222 (2018).
23. F.U. Enikeev and A.A. Kruglov, *Int. J. Mech. Sci.* 37, 473 (1995).
24. D. Sorgente, G. Palumbo, and L. Tricarico, *Key Eng. Mater.* 344, 119 (2007).
25. G. Palumbo, D. Sorgente, L. Tricarico, S.H. Zhang, W.T. Zheng, L.X. Zhou, and L.M. Ren, *Mater. Sci. Forum* 551–552, 317 (2007).
26. L.W.F. Mackenzie and M.O. Pekguleryuz, *Scr. Mater.* 59, 665 (2008).
27. A. El-Morsy, K. Manabe, and H. Nishimura, *Mater. Trans.* 43, 2443 (2002).
28. A. Akhtar and E. Teghtsoonian, *Acta Metall.* 17, 1339 (1969).
29. Y. Chino, M. Kado, and M. Mabuchi, *Acta Mater.* 56, 387 (2008).
30. C.H. Cáceres and A. Blake, *Phys. Status Solidi Appl. Res.* 194, 147 (2002).
31. C.H. Cáceres and A.H. Blake, *Mater. Sci. Forum* 567–568, 45 (2008).
32. N. Stanford and M.R. Barnett, *Magnesium Technology, 2012*, eds. S.N. Mathaudhu, W.H. Sillekens, N.R. Neelameggham, and N. Hort (Cham: Springer, 2016), pp. 207–211.
33. A.H. Blake and C.H. Caceres, *Mater. Sci. Eng. A* 484, 161 (2008).
34. J.F. Nie, Y.M. Zhu, J.Z. Liu, and X.Y. Fang, *Science* 340, 957 (2013).
35. S.L. Shang, W.Y. Wang, B.C. Zhou, Y. Wang, K.A. Darling, L.J. Kecskes, S.N. Mathaudhu, and Z.K. Liu, *Acta Mater.* 67, 168 (2014).